CHEMISTRY OF MATERIALS

ARTICLE

pubs.acs.org/cm

# Magnetotunable Hybrid Films of Stratified Iron Oxide Nanoparticles Assembled by the Layer-by-Layer Technique

Benoit P. Pichon,[†,*] Pierric Louet,[†,‡] Olivier Felix,[‡] Marc Drillon,[†] Sylvie Begin-Colin, and Gero Decher[‡,*]

[†]Institut de Physique et de Chimie des Matériaux de Strasbourg, Université de Strasbourg, UMR 7504 CNRS/UdS/ECPM, 23 rue du Loess — BP 23, 67034 Strasbourg Cedex 2, France

[‡]Institut Charles Sadron, Université de Strasbourg, CNRS UPR 22, 23 rue du Loess — BP 84047, 67034 Strasbourg Cedex 2, France

Supporting Information

**ABSTRACT:** Multilayer assemblies of iron oxide nanoparticles with tunable magnetic properties have been prepared by the layer-by-layer technique. The magnetic properties of multilayer assemblies depend closely on the stacking of nonagglomerated nanoparticles and, in particular, on the interlayer distance between nanoparticles, which is defined by the thickness of the polyelectrolyte multilayers. Therefore, the dipolar interactions between nanoparticles were demonstrated to occur preferentially in the plane of the nanoparticle layers and to result in the antiparallel magnetic coupling of adjacent nanoparticle layers, which is modulated as a function of the interlayer distance.

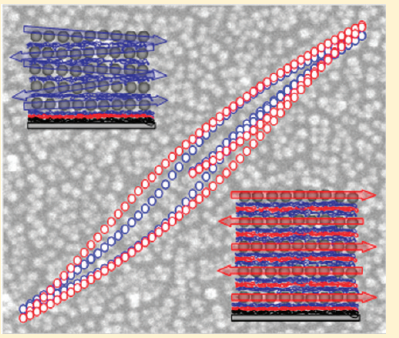

**KEYWORDS:** magnetic nanoparticle, layer-by-layer assemblies, dipolar interactions, iron oxide, nanostructure

## INTRODUCTION

Precise control of the physical properties of nanostructures is a challenging issue in the development of new devices for technological applications such as ultrahigh density magnetic recording,[1−3] magneto-optical devices or magnetoelectronic devices.[4,5] To this end, magnetic nanoparticles (NPs) assembled into two-dimensional (2D) or three-dimensional (3D) structures are very attractive because of their size[6] and morphology[7] dependent properties and high surface/volume ratio when compared to bulk materials. Bottom-up approaches including self-assembling methods have been demonstrated to be very efficient in the design of stable nanostructures based on nanoparticles. The choice of the assembling method is key to the control of the structural properties of NP assemblies and, accordingly, their magnetic properties. Indeed, magnetic monodomain nanoparticles are featured by a single magnetic moment and can be assimilated to elemental nanomagnets, which interact together through dipolar interactions. Recently, considerable attention has been directed to studies of magnetic NPs assembled in arrays because of their tunable magnetic properties. Indeed, dipolar interactions influence directly the magnetic properties of nanoparticles assemblies and can be finely tuned by controlling the spatial arrangement and interparticle distance. Due to its control of lateral pressure, the Langmuir—Blodgett technique is well suited for preparing dense monolayers or multilayers of organized NPs with strong magnetic interactions between them and collective properties.[8−11] In 2D assemblies, dipolar interactions were shown to be oriented preferentially in the plan of the film, while in 3D assemblies they are disoriented as a consequence of interactions between adjacent layers.[12] In contrast, the self-assembled monolayer (SAM) directed assembly technique, which enables the fine-tuning of surface functionalization, is more suitable to assemble NPs into 2D sizable domains with original collective properties.[13,14] The strength of dipolar interactions was demonstrated to increase with the size of NP assemblies, while for clusters of less than four nanoparticles they were very weak.

Among these approaches, the layer-by-layer (LbL) technique displays great potential for magnetic applications because multilayered architectures can be prepared on extended areas with controlled structure and thickness. As a very simple method to process, the construction of multilayered films is based upon the alternative deposition of oppositely charged entities. Initially developed with micrometer-sized colloids, the high potential of the LbL technique was demonstrated by using polyelectrolytes[15] and further extended to nanoparticles[16] with biological,[17] mineral,[18] semiconductor,[19] and metallic[20] properties. Hybrid assemblies of alternating polymers and iron oxide nanoparticles have also been reported for the development of magnetic resonance imaging (MRI) guided therapy,[21] adsorbents,[22,23] micromanipulators,[23] sensors,[24,25] and microactuators.[26,27]

Although the LbL technique has been applied to many systems, the preparation of multilayer assemblies with high control over the distance between NP layers has been poorly reported. Distance dependent properties as a function of the layer separation have been demonstrated in pioneered work on enzymatic activity.[28] The increase in the interlayer distance between enzymes layers in LbL assemblies favored catalytic activity. This approach has also been used to control the plasmon resonance of gold nanoparticle multilayer assemblies prepared by

**Received:** April 21, 2011
**Revised:** July 1, 2011
**Published:** July 27, 2011

LbL spin coating.[29] In another study, the strong distance dependent fluorescent quenching of gold nanocolloids was shown by controlling the layer thickness of nonfluorescent polyelectrolytes assembly separating fluorescent labeled polymers from the surface of gold NPs.[30]

Despite the great potential of using structured NP assemblies in future applications in magnetics, the use of hierarchical architectures for the enhancement of magnetic properties is still a fledgling field. Layer-by-layered assemblies of iron oxide NPs coated with a polyelectrolyte,[27] an insulating $SiO_2$ layer,[31] or stratified by clays[32,33] have been reported earlier with the aim of tuning the magnetic properties of films. Conducting polymers were also used to study magneto-transport properties.[34−36] However, in these studies, iron oxide NPs were prepared by the coprecipitation method that produces NPs in aqueous media with substantial fractions of aggregated NPs that are difficult to remove or to disaggregate. Assemblies based on such aggregated NPs display low ordering and are often hampered by a low tunability of their magnetic properties because dipolar interactions are very sensitive to interparticle distances in any type of spatial arrangement.[37] As a result, the fine control of magnetic properties of such hybrid nanostructures can only be fully accomplished in systems composed of nonaggregated nanoparticles. Only a few studies were conducted on well-defined layer-by-layer assemblies based on nonaggregated iron oxide NPs. Although these NPs were commercial products and were poorly characterized, the mechanism of the assembling process and the structure of such multilayer films has been recently investigated by ellipsometry[38] and neutron reflectometry.[39] Magnetic interactions have also been used to accelerate the deposition of subsequent layers of iron oxide by applying an external magnetic field during the assembling process.[40] Stable suspensions of FePt nanoparticles in organic solvents have also lead to improved nanoarchitectures and showed potential in the tuning of magnetic properties.[41,42]

Recently, syntheses involving the thermal decomposition of iron complexes have led to the preparation of stable suspensions of nonagglomerated nanoparticles because of in situ coating by surfactant molecules.[6,43] This synthesis method has opened new opportunities toward the assembling of iron oxide nanoparticles and the fine control of magnetic properties. Here, we report on the magnetotunable properties of well-defined nanostructures that consist of iron oxide nanoparticle assemblies prepared by the LbL technique. Such control results from the use of a stable suspension of nonagglomerated nanoparticles in an aqueous medium so obtained after performing phase transfer by ligand exchange. Such suspensions are expected to favor multilayer assemblies characterized by well-defined distances between the NP layers and accordingly tuned magnetic interactions. We demonstrate that the magnetic properties depend closely on the stacking of nonagglomerated NPs and in particular on the superlattice spacing within the polyelectrolyte multilayer architecture, i.e., the number of polyanion/polycation layer pairs separating the NP monolayers.

## EXPERIMENTAL SECTION

**Chemicals.** Citric acid (99.0%) and potassium citrate (99.5%) were purchased from Alfa Aeser. Polyethylene imine (PEI), poly(allylamine hydrochloride) (PAH), and poly(sodium 4-styrenesulfonate) (PSS) were purchased from Roth. Ultra pure water (Barnstead EASYpure LF system; R >17.7 MΩ.cm) and Milliq Gradient System (Millipore, Molsheim, France) was used for preparing the aqueous solutions and rinsing procedures.

**Ligand Exchange.** Twelve nanometer-sized nanoparticles coated with oleic acid were synthesized as reported previously.[6,10] The replacement of the hydrophobic coating was performed by phase transfert: 15 mL of a suspension of NP@ole with a concentration of 1 $mg.mL^{-1}$ was introduced in a vial. 15 mL of a buffer solution of citric acid (0.133 g) and potassium citrate (0.377 g) at pH 5 were added carefully. After 24 h at room temperature, the phase transfer operated under static conditions. The organic phase at the bottom in the vial became clearer as the aqueous upper phase became brownish. The NP@cit suspension was obtained after filtration on 100 nm pore filters mounted on a syringe.

**Preparation of Hybrid Films.** Hybrid films were deposited on single polished (100)-oriented single crystalline silicon wafers (500 $\mu$m thick, 1 cm wide, and 5 cm long), which were used after cleaning in a mixture of methanol and chlorhydric acid (37%) (50/50, v/v) for 30 min followed by immersing in sulphuric acid for 12 h. Solutions of polyelectrolyte were prepared as follows: PEI (250 mg) was dissolved in water (100 mL), PAH (71.5 mg) and NaCl (2.94 g) in water (250 mL), and PSS (154.5 mg) and NaCl (2.94 g) in water (250 mL). Polyelectrolyte multilayers were applied by spraying as well as rinsing stages (10 s) with water after each deposition of polyelectrolyte. First, a multilayer of PEI/PSS/PAH was deposited, followed by dipping into the suspension of NP@cit for 2 min. The rinsing procedure involves dipping in water three times (2, 1, and 1 min, respectively) followed by drying under a stream of nitrogen. Then, PAH or PAH/$(PSS/PAH)_6$ layers were deposited alternatively with NP@cit to produce packed and separated architectures.

**Characterization of NPs and NP Assemblies.** Transmission electron microscopy (TEM) was performed using a TOPCON model 002B microscope operating at 200 kV with a point-to-point resolution of 0.18 nm. Dynamic light scattering (DLS) measurements and $\zeta$ potential analyses were performed using a Zetasizer nano-SZ (Malvern Instruments). Scanning electron microscopy (SEM) was performed using a JEOL 6700 microscope equipped with a field emission gun (SEM-FEG) operating at an accelerating voltage of 3 KV. Ellipsometry measurements were performed with a plasmon SD 2300 ellipsometer operating at the single wavelength of 632.8 nm and a constant angle of 70°. UV−vis spectra were recorded with a Varian Cary 500 scan spectrophotometer. Atomic force microscopy (AFM) was performed using a Digital Instrument 3100 microscope coupled to a Nanoscope IIIa controller. Measurements were done in the tapping mode on substrates before and after exposure to the suspension of nanoparticles. Collected data were analyzed with Nanotec WSXM software.[44]

**Magnetic Characterization of NP Assemblies.** The magnetic properties of the assemblies and NPs in the powder state were studied with a superconducting quantum interference device (SQUID) magnetometer (Quantum Design model MPMS-XL). Magnetization curves were recorded at 300 K and 5 K as a function of an external magnetic field applied in a parallel (in-plan) or perpendicular (out-of-plan) direction to the plane of the surface. They were scaled as a function of the saturation magnetization. Zero-field-cooled (ZFC) and field-cooled (FC) curves were recorded as a function of the temperature from 5 to 300 K under exposure to a magnetic field of 75 G applied in-plane. ZFC curves were first recorded from 5 to 300 K without applying any magnetic field upon the decrease in the temperature. Then, the FC curves were recorded after reducing the temperature again to 5 K under a magnetic field of 75 G.

## RESULTS AND DISCUSSION

A prerequisite for the present study is the preparation of a highly stable aqueous suspension of nonaggregated iron oxide NPs. Iron oxide nanoparticles (NP@ole) exhibiting a diameter of 10 nm and the spinel structure and coated with oleic acid molecules were synthesized according to the decomposition

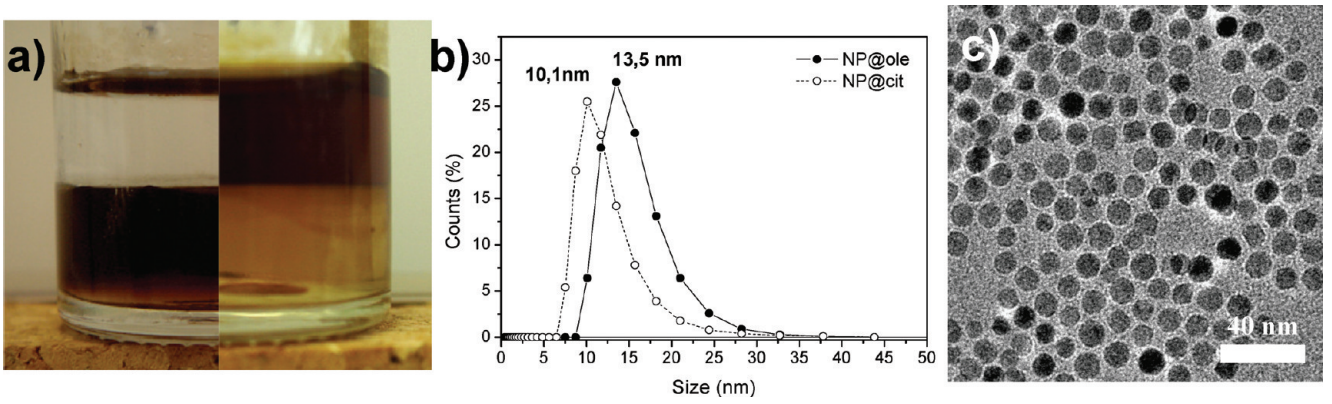


**Figure 1.** (a) Photograph of NP suspensions before (left) and after (right) phase transfer and (b) DLS size distributions by volume of NP@ole and NP@cit suspensions. (c) TEM micrograph of NP@cit after ligand exchange.

**Scheme 1. Idealized Representations of Packed Architecture $(NP/PAH)_5$ and Well-Separated Architecture $(NP/PAH(PSS/PAH)_6)_5$ Each Comprised of Five Layers of Iron Oxide NPs**

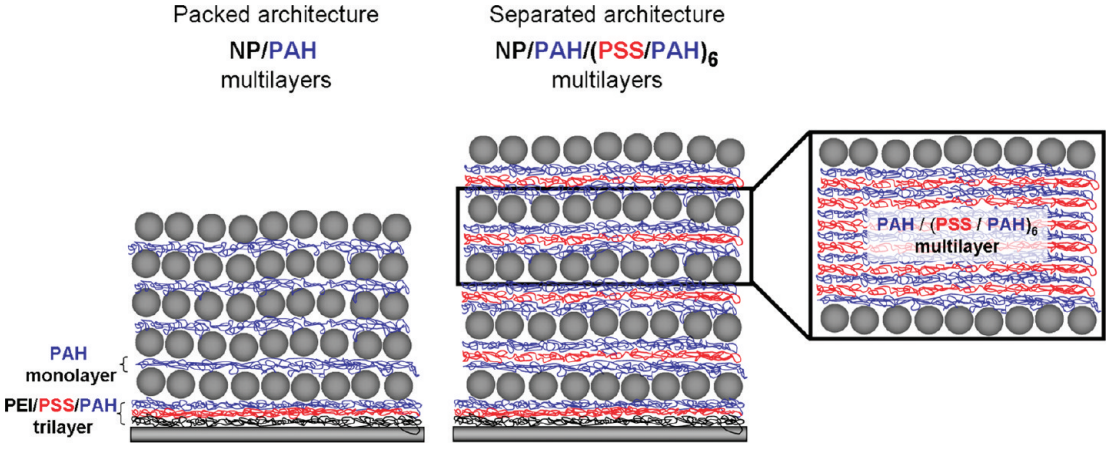


method.[6,7,10,46] Although NP@ole are highly stable in organic solvents such as chloroform, they are not well suited for LbL assembly because of their lack of surface charge. Therefore, a ligand exchange reaction was performed by phase transfer of NPs from a chloroform solution to an aqueous buffer mixture of potassium citrate and citric acid (0.15 M, pH 5). Panel (a) of Figure 1 shows the respective change of color of both the chloroform and aqueous solutions after 12 h under static conditions, which clearly demonstrates the success of ligand exchange procedure. The citrate coated NPs (NP@cit) thus obtained remain highly stable in aqueous media, most likely because of their zeta potential of −32 mV. Dynamic light scattering (DLS) results indicated that the ligand exchange proceeds without appreciable aggregation of the NPs (Figure 1b). Before the ligand exchange, the hydrodynamic diameter of 13.5 nm as measured by DLS is in good agreement with the 10.0 ± 1.3 nm sized NP cores surrounded by a 2 nm shell of oleic acid as observed by transmission electron microscopy (TEM) (Figure 1c). The decrease in this value to 10.1 nm for the aqueous suspension of NP@cit after the ligand exchange confirms the removal of oleic acid and its replacement by the much smaller citrate molecule. Infrared spectroscopy also confirms these observations that show the decrease in intensity of the $\nu$C−H band and the increase in intensity of the $\nu$C═O bands with respect to the $\nu$Fe−O band (Supporting Information).

Subsequently, hybrid superlattice nanostructures were prepared by incorporating negatively charged NP@cit into poly(allylamine hydrochloride) (PAH) and poly(sodium 4-styrenesulfonate) (PSS) multilayers. Polyelectrolytes were deposited by spraying onto a silica wafer, whereas NP@cit were absorbed on the terminating PAH layer by dipping the sample into a stable suspension of the NPs. The deposition conditions for NP@cit were optimized, and the highest surface coverage was obtained after dipping the sample for 2 min. Two architectures with different interlayer distances were prepared with the aim of studying the influence of the nanostructure on the magnetic properties (Scheme 1): (i) packed architectures of NP monolayers alternating with only one layer of PAH (NP/PAH) and (ii) well-separated architectures of NP monolayers alternating with six PSS/PAH layer pairs ($NP/PAH(PSS/PAH)_6$). In the latter, the six PSS/PAH layer pairs, which roughly correspond to a thickness of 10 nm, are expected to reduce the roughness induced by the NP monolayer and lead to better control over the arrangement of additional NP layers. Furthermore, model calculations with 10 nm diameter spherical iron oxide NPs show that the influence of dipolar interactions is much

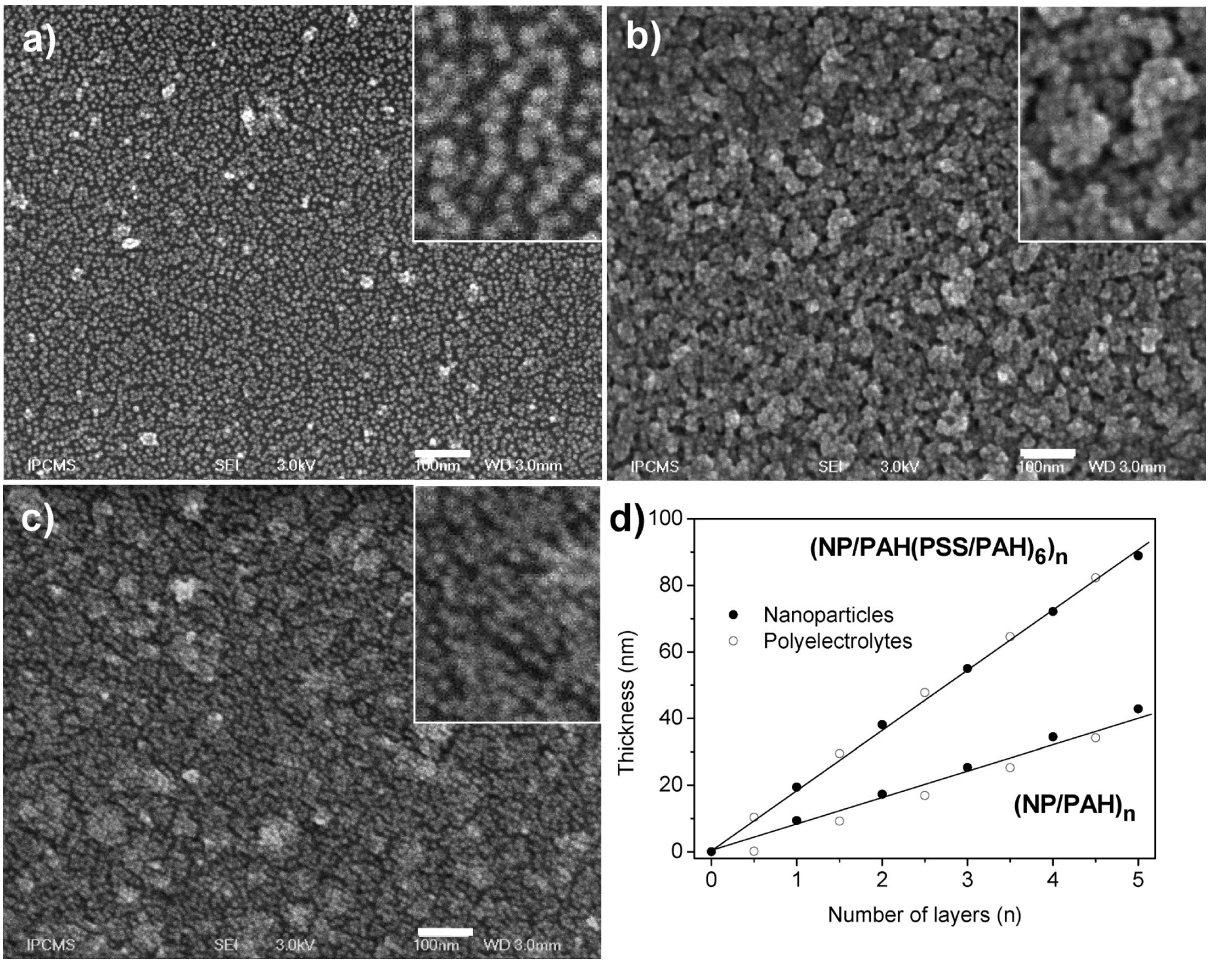


**Figure 2.** SEM images after deposition of (a) the first layer of NP@cit, (b) packed $(NP/PAH)_5$, and (c) separated $(NP/PAH(PSS/PAH)_6)_5$ architectures. Scale bars are 100 nm. (d) Evolution of the film growth for close contact $(NP/PAH)_n$ and well- separated $(NP/PAH(PSS/PAH)_6)_n$ multilayer architectures as determined by ellipsometry.

weaker than the anisotropy field for particle separations greater than 10 nm.[45] Therefore, the six PSS/PAH layer pairs are expected to have influence on the dipolar interactions between NP layers in comparison to only one PAH layer. For both architectures, ellipsometry measurements showed that the thickness increases linearly with the number of deposition cycles (Figure 2d). The regular deposition of NP layers with a thickness of $7.0 \pm 1.4$ and $7.4 \pm 1.6$ nm for packed and separated architectures, respectively, is in good agreement with the measured thickness of spherical 10 nm sized NP layers (Supporting Information). Moreover, in the separated architecture, the thickness of the six PSS/PAH layer pairs ($10.1 \pm 0.3$ nm) is remarkably constant.

The surface morphology of both architectures containing five NP layers was investigated by scanning electron microscopy (SEM). These were compared to the first layer of NPs before subsequent depositions, which is characterized by a dense and homogeneous coverage of the surface with almost no aggregates in comparison to previous studies (Figure 2a). Upon closer investigation, it can be seen that NPs tend to arrange themselves into small domains (inset), which may be related to dipole−dipole interactions between nanoparticles.[46] After deposition of five PAH/NPs layer pairs, aggregated NPs are observed (Figure 2b), whereas five NP layers separated by six PSS/PAH layer pairs produce a more homogeneous surface morphology (Figure 2c). These observations are corroborated by height images and the corresponding cross-section panels recorded by atomic force microscopy (AFM) (Figure 3). The well-separated layer architecture unambiguously displays finer grain texture than that of the packed layer architecture, which exhibits aggregates that increase in size as the number of NP layers increases. Moreover, the mean roughness (Ra) of the packed layer architecture (6.7 nm) is higher than that for the well-separated case (3.1 nm). Although these values are larger than that of the first NP layer (2.1 nm), they remain very low in comparison with those reported previously.[38] In the packed architecture, the formation of aggregates is attributed to the roughness propagation induced by inner NP layers, which is impossible to smooth out by a single layer of PAH polyelectrolyte. In contrast, in well-separated layer architectures, the deposition of six PAH/PSS layer pairs reduces the surface roughness and regenerates a much smoother surface, which limits the formation of such aggregates.[39] Therefore, well-defined NP monolayers are formed. These results demonstrate the preparation of 3D assemblies with a high control over the distance between NP monolayers.

Magnetic properties of the packed and well-separated layered architectures were investigated by using a SQUID magnetometer and were compared to a powdered sample of NP@cit. M(H) curves have been scaled to the saturation magnetization (Ms) in order to

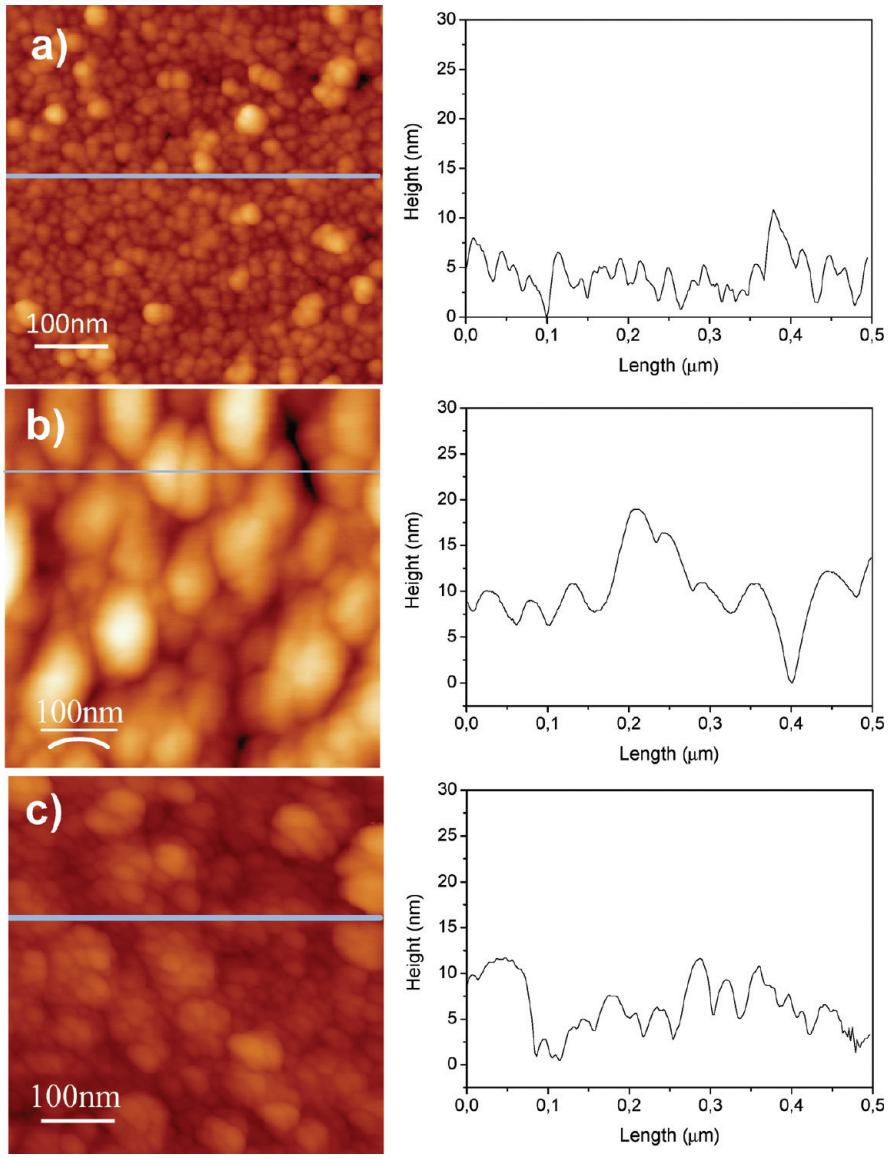


**Figure 3.** AFM images after deposition of (a) the first layer of NP@cit, (b) packed $(NP/PAH)_5$ architecture, and (c) separated $(NP/PAH(PSS/PAH)_6)_5$ architecture. Height image (left) and profile (right) are indicated by the line in the corresponding height image.

compare them (Figure 4a,b). For all samples, M(H) curves measured at 300 K by applying a magnetic field in the plane of the film exhibit superparamagnetic behavior. In turn, the samples show hysteretic behaviors at 5 K, which is consistent with a very slow relaxation of the magnetic moment. The coercitive fields for packed (Hc = 370 Oe) and well-separated (Hc = 350 Oe) layered architectures are similar to the random NP@cit assembly (Hc = 420 Oe) and do not allow any comparison between both assemblies because in the latter the Hc value fluctuates from one sample to the other.

The magnetic anisotropy in both the packed and the well-separated layer architectures can be determined from magnetic experiments using an applied field direction parallel (in-plane) and perpendicular (out-of-plane) to the film. The squareness of the hysteresis loop, defined as Mr/Ms, gives some insight into the strength of the dipolar interactions between NPs, which for a layered structure are expected to align magnetic moments in-plane and therefore to promote a ferromagnetic 2D ordering. Very clearly, the situation becomes more complicated when a small out-of-plane anisotropy exists or when the NP layers are close enough to interact because, depending on the competing influences of these effects, a ferro or antiferromagnetic ordering may take place. It is observed that packed and well-separated layer architectures exhibit similar Mr/Ms ratios of 0.47 and 0.43, respectively, for the in-plane magnetic field, while these values are twice as small, 0.22 and 0.26, respectively, when the field is out-of-plane (Figure 4a,b). These findings clearly demonstrate that the magnetic moments of the NPs are preferentially oriented parallel to the plane of the film. In comparison, randomly assembled NP@cit display a Mr/Ms ratio of 0.27 and higher saturation field that corresponds to individual NP magnetic moments with random orientation in space, as reported by Poddar *et al.*[12] In this case, the external field competes with dipolar interactions to align magnetic moments along the applied direction.

A better insight into the low-temperature magnetic properties of both architectures is provided by application of a low out-of-plane


dx.doi.org/10.1021/cm201139s |*Chem. Mater.* 2011, 23, 3668–3675

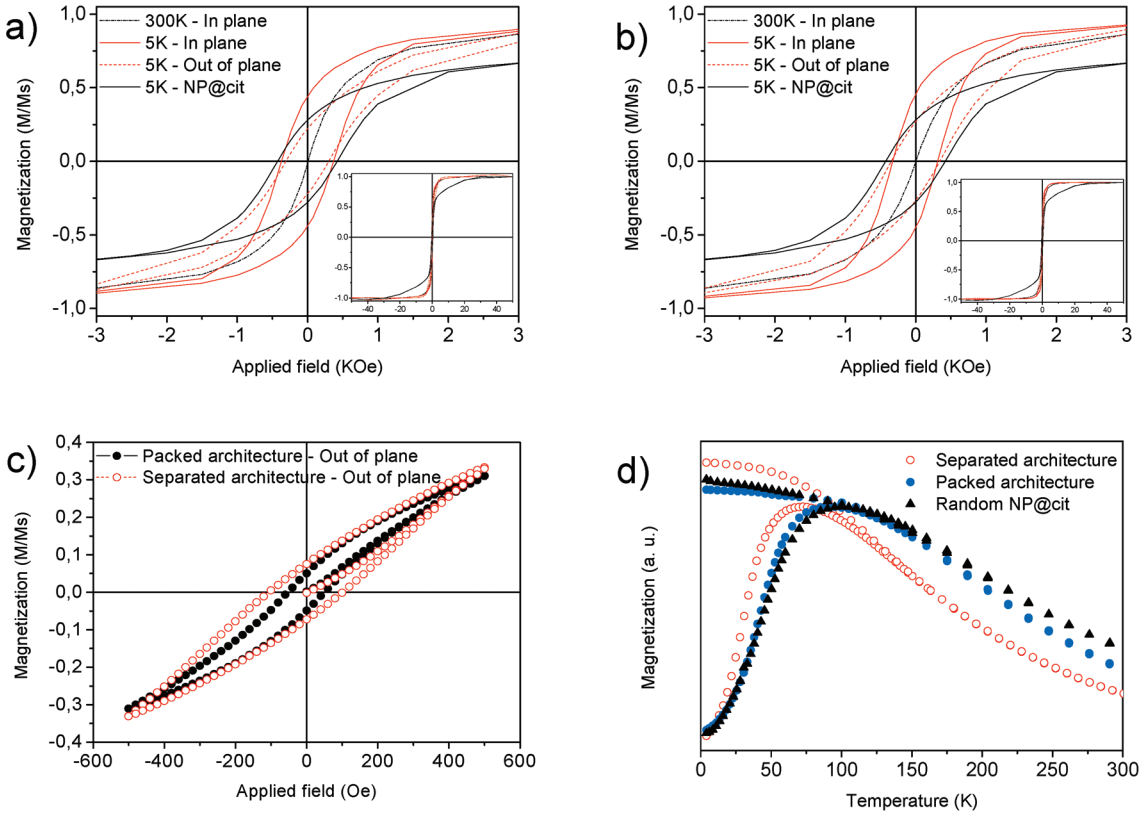


**Figure 4.** Magnetization curves of five multilayer films following the packed (a) and separated (b) architectures compared to NP@cit in the powdered state. The magnetic field was applied in the parallel (in-plane) and in perpendicular (out-of-plane) directions to the plane of the NP films. Insets are enlargements of the curves from −50 to 50 KOe. (c) Out-of-plane magnetization curves of both architectures recorded in the −500 to 500 Oe range. (d) ZFC/FC curves.

magnetic field, ranging from +500 Oe to −500 Oe (Figure 4c). First, it can be seen that the magnetization curves differ significantly from those recorded in high fields (Figure 4a,b). The M(H) plots for both of the architectures agree with a harder alignment of magnetic moments along H when the layers are far from each other. The first magnetization curve of the well-separated layer system, which varies linearly up to about 150 Oe, points to an antiparallel magnetization of neighboring NP layers, most likely due to a small, but non-negligible, interlayer dipolar coupling. In turn, the behavior of the packed layer system is more conventional and better described by an out-of-plane component of the magnetization.

Zero-field-cooled (ZFC) and field-cooled (FC) magnetization curves (Figure 4d) were scaled to the same asymptotic high temperature value because the Curie constant does not depend on the NP arrangement. They reflect the occurrence of a freezing of the NP magnetic moment at $T_B$ (located at the ZFC maximum), and the fact that dipolar interactions between NP layers play a significant role as well. Thus, the $T_B$ value (72 K) for well-separated NP layers is significantly lower than that observed for the packed NP layers and random NP@cit samples (93 and 100 K, respectively), which highlights the influence of dipolar coupling over very large distances. In addition, the ZFC curves of the packed NP layers and random NP@cit samples exhibit the largest broadening, which indicates that the mechanism of freezing depends on the arrangement of nanoparticles.

It is well documented that a long-range ordering may occur at high temperatures in layered systems composed of strongly correlated spin-1/2 separated by organic species, even for interlayer spacings as large as a few nanometers.[47,48] Of course, as far as single spins are concerned, the strength of the dipolar interaction remains very weak. However, as the dipolar energy depends on the square of the effective moment, the interaction between blocks of parallel spins become significant. As a result, dipolar interactions cannot be ignored in low-dimensional ferromagnets made of an assembly of chains or layers where the spins are correlated over larger and larger distances as T decreases or as in NP-based materials where the magnetic moment is blocked below $T_B$. In the iron oxide NPs under consideration, the interaction calculated using the point dipole approximation model is about $10^8$ times larger than between elementary spin-1/2 for the same distance, which is a leading effect.

Considering the two types of assembly investigated here—well-separated layers with a basal spacing of 16.5 nm and packed layers with a basal spacing of 8.6 nm— it is clear that the increase in the interlayer distance is a major factor influencing the magnetic behavior. For the former, the in-plane anisotropy dominates because of dipolar interactions within layers, and the interlayer coupling which is expected to be much smaller tends to stabilize an antiparallel alignment of the layer moments. The interlayer dipolar coupling is highlighted in the M(H) curve at low fields perpendicular to the film. Unlike quantum systems, no spin-flip is observed because of the giant magnetic moment of NPs ($>10^4$ $\mu$B). For the packed layer architecture, even though NPs always interact preferentially in-plane, the shape of the M(H) curve points to a non-negligible out-of-plane component


dx.doi.org/10.1021/cm201139s |*Chem. Mater.* 2011, 23, 3668–3675

of the magnetization as a result of strong interlayer dipolar coupling. The influence of this coupling is further evidenced from the significant increase in $T_B$ as the interlayer distance is shortened from 10 to 1 nm between the well-separated and packed layer architectures. For the packed architecture, it should be emphasized that even though the elementary unit is the magnetic NP characterized by a blocking temperature $T_B$, the behavior is likely more representative by considering the weight of dipole−dipole interactions that favor magnetic ordering and lead to the increase in $T_B$ from 72 to 93 K. The randomly assembled NP@cit sample exhibits a further increase in $T_B$ (up to 100 K) that may be explained by the shorter interparticle distance due to citrate molecules on the NP surface.

## CONCLUSIONS

In summary, we have demonstrated the ability to finely tune the magnetic properties of iron oxide NP assemblies by controlling the formation of the LbL nanostructure. The use of a highly stable suspension of nonaggregated iron oxide NPs enables the preparation of well-defined nanostructures. Therefore, hierarchical architectures based on the assembling of NP monolayers with very low roughness combined with the precise control of the interlayer distance by polyelectrolyte layer pairs enables the control of the magnetic properties of the film. To the best of our knowledge, this is the first time that stable suspensions of nonaggregated iron oxide NPs in an aqueous medium were used to tune the magnetic properties of well-defined nanostructures prepared by the LbL technique. In this study, we demonstrated that iron oxide NPs interact preferentially in the plane of the NP layers through dipolar interactions. Furthermore, we demonstrated that the resulting strong magnetic anisotropy along each NP layer induces their antiparallel coupling. Such coupling is highly dependent on the dipolar interactions that occur between NPs of adjacent layers. Therefore, the fine control of the distance between NP layers by adjusting the thickness of the polyelectrolyte layer leads to the modulation of the magnetic properties of these assemblies. The approach, which is easy to implement in a manufacturing process, should bring new and promising developments to the preparation of devices in nanoelectronics.

## ASSOCIATED CONTENT

**Supporting Information.** FTIR spectra, ellipsometry data, magnetization curves. This information is available free of charge via the Internet at http://pubs.acs.org/.

## AUTHOR INFORMATION

### Corresponding Author

*E-mail: Benoit.Pichon@unistra.fr. Fax: 0033 (0)3 88 10 72. Tel.: 0033 (0)3 88 10 71 33.

## ACKNOWLEDGMENT

This work was supported by the project ANR08-BLAN-NT09-459731, "MAGARRAY" from the Agence Nationale de la Recherche (ANR). G. Decher is indebted to the Institut Universitaire de France (IUF) and to the International Center for Frontier Research in Chemistry (icFRC) for financial support.

## REFERENCES

(1) Osada, M.; Ebina, Y.; Takada, K.; Sasaki, T. *Adv. Mater.* **2006**, *18*, 295.
(2) Reiss, G.; Hutten, A. *Nat. Mater.* **2005**, *4*, 725.
(3) Thomson, T.; Abelmann, L.; Groenland, J. P. J. Magnetic Data Storage: Past, Present and Future. In *Magnetic Nanostructures in Modern Technology*; Springer: Berlin, 2007.
(4) Dayen, J.-F.; Faramarzi, V.; Pauly, P.; Kemp, N. T.; Barbero, M.; Pichon, B. P.; Majjad, H.; Begin-Colin, S.; Doudin, B. *Nanotechnology* **2010**, *21*, 335503.
(5) Zeng, H.; Black, C. T.; Sandstrom, R. L.; Rice, P. M.; Murray, C. B.; Sun, S. *Phys. Rev. B* **2006**, *73*, 020402.
(6) Demortière, A.; Pichon, B.; Panissod, P.; Donnio, B.; Pourroy, G.; Guillon, D.; Bégin-Colin, S. *Nanoscale* **2011**, 225–232.
(7) Pichon, B. P.; Gerber, O.; Lefevre, C.; Florea, I.; Fleutot, S.; Baaziz, W.; Pauly, M.; Ohlmann, M.; Ulhaq, C.; Ersen, O.; Pierron-Bohnes, V.; Panissod, P.; Drillon, M.; Begin-Colin, S. *Chem. Mater.* **2011**, *23*, 2886–2900.
(8) Fried, T.; Shemer, G.; Markovich, G. *Adv. Mater.* **2001**, *13*, 1158.
(9) Mammeri, F.; Bras, Y. L.; Daou, T. J.; Gallani, J.-L.; Colis, S.; Pourroy, G.; Donnio, B.; Guillon, D.; Begin-Colin, S. *J. Phys. Chem. B* **2008**, *113*, 734.
(10) Pauly, M.; Pichon, B. P.; Demortière, A.; Delahaye, J.; Leuvrey, C.; Pourroy, G.; Bégin-Colin, S. *Superlattices Microstruct.* **2009**, *46*, 195.
(11) Pauly, M.; Pichon, B. P.; Albouy, P. A.; Fleutot, S.; Leuvrey, C.; Trassin, M.; Gallani, J. L.; Begin-Colin, S. *J. Mater. Chem* **2011**, DOI: 10.1039/c1jm12012c.
(12) Poddar, P.; Telem-Shafir, T.; Fried, T.; Markovich, G. *Phys. Rev. B* **2002**, *66*, 060403.
(13) Pichon, B. P.; Demortiere, A.; Pauly, M.; Mougin, K.; Derory, A.; Begin-Colin, S. *J. Phys. Chem. C* **2010**, *114*, 9041.
(14) Pichon, B. P.; Pauly, M.; Marie, P.; Leuvrey, C.; Begin-Colin, S. *Langmuir* **2011**, *27*, 6235–6243.
(15) Decher, G.; Hong, J. D.; Schmitt, J. *Thin Solid Films* **1992**, *210−211*, 831.
(16) Jiang, C.; Tsukruk, V. V. *Adv. Mater.* **2006**, *18*, 829.
(17) Lvov, Y.; Haas, H.; Decher, G.; Moehwald, H.; Mikhailov, A.; Mtchedlishvily, B.; Morgunova, E.; Vainshtein, B. *Langmuir* **1994**, *10*, 4232.
(18) Kleinfeld, E. R.; Ferguson, G. S. *Science* **1994**, *265*, 370.
(19) Kotov, N. A.; Dekany, I.; Fendler, J. H. *J. Phys. Chem.* **1995**, *99*, 13065.
(20) Schmitt, J.; Decher, G.; Dressick, W. J.; Brandow, S. L.; Geer, R. E.; Shashidhar, R.; Calvert, J. M. *Adv. Mater.* **1997**, *9*, 61.
(21) Wang, X.; Zhou, S. Y.; Lai, Y.; Sun, J. Q.; Shen, J. C. *J. Mater. Chem.* **2010**, *20*, 555–560.
(22) Shi, F.; Liu, S. H.; Gao, H. T.; Ding, N.; Dong, L. J.; Tremel, W.; Knoll, W. *Adv. Mater.* **2009**, *21*, 1927–1930.
(23) Wang, G. J.; Fang, Y. N.; Kim, P.; Hayek, A.; Weatherspoon, M. R.; Perry, J. W.; Sandhage, K. H.; Marder, S. R.; Jones, S. C. *Adv. Funct. Mater.* **2009**, *19*, 2768–2776.
(24) Zhang, L. H.; Zhai, Y. M.; Gao, N.; Wen, D.; Dong, S. J. *Electrochem. Commun.* **2008**, *10*, 1524–1526.
(25) Hua, F.; Cui, T.; Lvov, Y. M. *Nano Lett.* **2004**, *4*, 823.
(26) Xue, W.; Cui, T. *J. Nanosci. Nanotechnol.* **2007**, *7*, 2647.
(27) Yanjing, L.; Anbo, W.; Richard, O. C. *Appl. Phys. Lett.* **1997**, *71*, 2265–2267.
(28) Onda, M.; Lvov, Y.; Ariga, K.; Kunitake, T. *J. Ferment. Bioeng.* **1996**, *82*, 502.
(29) Jiang, C.; Markutsya, S.; Tsukruk, V. V. *Langmuir* **2004**, *20*, 882.
(30) Schneider, G.; Decher, G.; Nerambourg, N.; Praho, R. s.; Werts, M. H. V.; Blanchard-Desce, M. *Nano Lett.* **2006**, *6*, 530.
(31) Farkhad, G. A.; Miguel, A. C.-D.; Arif, M.; John, W. O.; Michael, G.; Lius, M. L.-M.; Nicholas, A. K. *Adv. Mater.* **1999**, *11*, 1006–1010.
(32) Mamedov, A.; Ostrander, J.; Aliev, F.; Kotov, N. A. *Langmuir* **2000**, *16*, 3941.
(33) Mamedov, A. A.; Kotov, N. A. *Langmuir* **2000**, *16*, 5530.
(34) Kim, H. S.; Sohn, B. H.; Lee, W.; Lee, J. K.; Choi, S. J.; Kwon, S. J. *Thin Solid Films* **2002**, *419*, 173–177.

(35) Paterno, L. G.; Soler, M. A. G.; Fonseca, F. J.; Sinnecker, J. P.; Sinnecker, E.; Lima, E. C. D.; Bao, S. N.; Novak, M. A.; Morais, P. C. *J. Nanosci. Nanotechnol.* **2010**, *10*, 2679–2685.
(36) Paterno, L. G.; Soler, M. A. G.; Fonseca, F. J.; Sinnecker, J. P.; Sinnecker, E.; Lima, E. C. D.; Novak, M. A.; Morais, P. C. *J. Phys. Chem. C* **2009**, *113*, 5087–5095.
(37) Demortière, A.; Buathong, S.; Pichon, B. P.; Panissod, P.; Guillon, D.; Bégin-Colin, S.; Donnio, B. *Small* **2010**, *6*, 1341.
(38) Grigoriev, D.; Gorin, D.; Sukhorukov, G. B.; Yashchenok, A.; Maltseva, E.; MÃ¶hwald, H. *Langmuir* **2007**, *23*, 12388.
(39) Kolasinska, M.; Gutberlet, T.; Krastev, R. *Langmuir* **2009**, *25*, 10292.
(40) Dey, S.; Mohanta, K.; Pal, A. J. *Langmuir* **2010**, *26*, 9627.
(41) Masayuki, S.; Yasuaki, E. *Angew. Chem., Int. Ed.* **2009**, *48*, 1754–1757.
(42) Sun, S.; Anders, S.; Hamann, H. F.; Thiele, J.-U.; Baglin, J. E. E.; Thomson, T.; Fullerton, E. E.; Murray, C. B.; Terris, B. D. *J. Am. Chem. Soc.* **2002**, *124*, 2884.
(43) Park, J.; An, K.; Hwang, Y.; Park, J.-G.; Noh, H.-J.; Kim, J.-Y.; Park, J.-H.; Hwang, N.-M.; Hyeon, T. *Nat. Mater.* **2004**, *3*, 891.
(44) Horcas, I.; Fernandez, R.; Gomez-Rodriguez, J. M.; Colchero, J.; Gomez-Herrero, J.; Baro, A. M. *Rev. Sci. Instrum.* **2007**, *78*, 013705.
(45) Ding, L.; Zhou, W.; Chu, H.; Jin, Z.; Zhang, Y.; Li, Y. Unpublished results.
(46) Kazuya, N.; Ying, H.; Oktay, U.; Osman, B.; Francesco, S. *Adv. Mater.* **2008**, *20*, 4294–4299.
(47) Drillon, M.; Panissod, P. *J. Magn. Magn. Mater.* **1998**, *188*, 93.
(48) Drillon, M.; Panissod, P.; Rabu, P.; Souletie, J.; Ksenofontov, V.; Gütlich, P. *Phys. Rev. B* **2002**, *65*, 104404.